Research Article

NUMERICAL INVESTIGATION OF THE EFFECT OF SECONDARY INLET PLACE ON THE FLOW PROPERTIES IN A CO-AXIAL BOUNDED JET

Salar IMANMEHR*[1], Iraj MIRZAEE[2], Nader POURMAHMOUD[3]

[1]*Department of Mechanical Engineering, Urmia University, Urmia, IRAN;* ORCID: 0000-0002-9405-8013
[2]*Department of Mechanical Engineering, Urmia University, Urmia, IRAN;* ORCID: 0000-0002-3523-5251
[3]*Department of Mechanical Engineering, Urmia University, Urmia, IRAN;* ORCID: 0000-0002-9974-6149

ABSTRACT

If a flow with a low thickness and high velocity enters a lower velocity fluid, the field of this interference is called jet stream. In the present manuscript, because of the importance of the turbulent co-axial jets, a numerical study is done on this kind of jets. In many jet systems, a high-speed fluid from a circular nozzle and a secondary fluid from a ring shaped nozzle co-axial with first nozzle at a lower speed is discharged into the tube. These two flows are mixed inside a tube and form a single stream. In this manuscript, in order to study the behavior of coaxial jets, the results of the computational fluid dynamics (CFD) are presented to determine the place of secondary inlet position on the suction ration. For this aim, different secondary inlets were simulated numerically by Computational Fluid Dynamics (CFD) software i.e. Fluent^{TM}. The obtained results showed that the appropriate place to create the secondary inlet is near the first inlet i.e. for the $\dfrac{\Delta r}{r} = 0.6$, one can achieve the highest amount of suction ratio in the jet. In addition the present CFD results were compared to the available experimental data which shows a good agreement.
Keywords: Turbulence jet, axial velocity, computational fluid dynamics, secondary inlet.

1. INTRODUCTION

High-pressure water jets are used in several trades secondary to their ability to generate high pressure fluid columns, however these same abilities can also confer a risk of severe penetrating injuries to patients. High pressure water jet injury to the oropharynx is rate with only 3 other reports of this type of injury [1, 2]. Up to now, Jets have been used as a variety of machining tools for pitting, surface texturing, perforating, cutting, milling, polishing, grooving, turning, and making complicated structures, etc [3, 4].

Chin et al. [5] numerically and experimentally investigated the forced convection heat transfer inside a rectangular channel for determining fluid flow and heat transfer properties. They also compared the performance of heat sinks with solid and perforated pins and showed that by increasing the number of perforations and their diameter, pressure drop decreases and the Nusselt number increases. In their experiments, thermal performance of the heat sink with perforated pins

---

* Corresponding Author: e-mail: salar.imanmehr1397@gmail.com, tel: +989144414178

was better than with solid pins. Nafon and Nakharintr [6] experimentally studied the effects of inlet temperature, Reynolds number, and heat flux on heat transfer properties of a water/TiO_2 nanofluid jet in a semi-rectangular heat sink, and showed that the average heat transfer coefficient of nanofluid is higher than base fluid, and the pressure drop increases by increasing the nanoparticle volume fraction. Jasperson et al. [7] studied the thermal and hydrodynamic performance of a copper microchannel and a pin fin microchannel and showed that by increasing the volume rate of flow, the thermal resistance of a pin fin heat sink decreases.

Forstall and Shapiro [8] measured the gaseous gas by injection of helium into the internal jet and using a gas sampling method in order to study the behavior of the co-axial gas jets. They used a Pitot tube to measure velocity. Starck [9] studied the flow field in a flame created by co-axial jets experimentally and measured mean velocity profiles at different axial distances. Morton [10] presented an analytical model for predicting velocity and concentration profiles. Due to the use of several basic assumptions, his model's consistency with experimental data was weak. Chigier and Beer [11] experimentally studied the near-nozzle area in higher than average air-to-air coaxial jet with the ratio of the external jet to the internal jet higher and lower than one. Ghodsian et al. [12] experimentally investigated the local scour due to free fall jets. They studied various values of the densimetric Froude number, the relative tailwater depth, the relative drop height and the relative sediment size. Their findings show that by increasing the sediment non-uniformity parameter the scour hole parameters decrease. Champagne and Wygnanski [13] measured the mean velocity, turbulence intensity and shear stress in air-to-air coaxial jets using a hot wire speedometer (HWS). Ribeiro and Whitelaw [14] experimentally studied the turbulent mixing in the developing area of coaxial jets in two swirl and non-swirl states. Ko and Kwan [15] used pressure gauges, hot wire and microphone spectrum to understand the structure of vortices in the near-nozzle area in coaxial jets. Dahm et al. [16] directly depicted the dynamics and structure of vortices in coaxial water-water jets using two-color plate laser-induced fluorescence (PLIF). Buresti et al. [17] determined the flow field of the coaxial air-air jets with the aid of the Laser-Doppler hot wire Speedometer (LDS). They investigated two different wall thicknesses of the internal circular nozzle in their research. Warda et al. [18] studied the effect of different parameters such as spraying speed on the flow field of air-to-air coaxial jets using a Laser-Doppler speedometer. Schumaker [19] did a comprehensive study of the flow of coaxial turbulent jets in a cold state (without reaction), and in the case of a reaction experiment. Zhuang et al. [20] studied heat transfer inside a microchannel with fluid jet and different coolants and showed that using fluid jet results in higher heat transfer compared with ordinary parallel flows.

The above articles are examples of researches on turbulent coaxial jet. However, no simple equations have been established to determine the velocity field. In this manuscript, in order to study the behavior of coaxial jets; the results of the computational fluid dynamics (CFD) are presented to determine the place of secondary inlet position on the suction ration.

2.1. Model Description

In this paper, a numerical model for studying the jet behavior is presented due to the importance of turbulent coaxial jets in a wall-bounded area. According to Fig. 1, consider a jet to be discharged into the pipe. The diameter of the input orifice is considered d and the diameter of the main tube is considered D.

According to Figure 1, there are three regions. The main goal of the present research is to obtain the mathematical equations of the velocity profile in the second and third regions and compare it with the experimental results of Liu et al. [21]. The first region is from the orifice to the end of the potential core (about 5d), in which the flow velocity is approximately equal to the velocity of the orifice output flow. Also, note that the output velocity of orifice is considered uniformly. The lower potential core is the second region, which is called Self-Preservation. The velocity profile in this region is similar to the velocity profile of the free jets. In both of these

areas, the reversed flow is observed near the walls. The third region starts from the point where the reversed flow is disconnected and the width of the jet is equal to the diameter of the pipe. In this area, the effects of the wall are more effective and the flow has the flow behavior inside the tube.
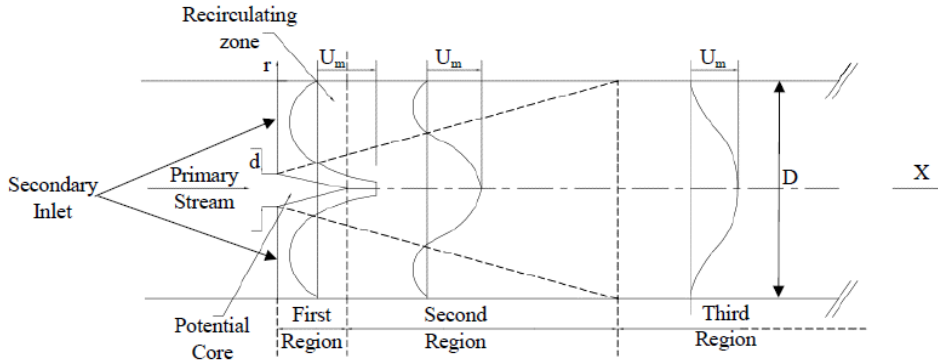
Figure 1. Schematic of jet discharged into a tube with diameter of D [21]

In this paper, we will try to study a jet with the secondary flow suctioned from the harness. In fact, we have two coaxial flows, the internal flow being the primary flow and the external current is called the secondary one. These two flows are mixed inside a tube and form a single flow. The temperature of both flows is considered to be the same. The primary flow speed is greater than the secondary flow (suction). Due to the symmetry of coaxial jets around their axis, these jets can be analyzed in two-dimensional form [22].

2.2. Governing Equations

The numerical model of jet is created using Gambit software in order to produce the computational network and Fluent 6.3.26 software package for solution the governing equations by control volume method in a two-dimensional incompressible and turbulence field [23, 24]. The present study uses the model of Liu et al. [21] which governing equations for the flow field process are as follows:

Differential form of the continuity equation:

$$\frac{\partial u}{\partial x} + \frac{\partial v}{\partial y} = 0 \tag{1}$$

Differential form of the momentum equation in x and y directions in the present research:

$$\rho(u\frac{\partial u}{\partial x} + v\frac{\partial u}{\partial y}) = -\frac{\partial P}{\partial x} + \mu\nabla^2 u \tag{2}$$

$$\rho(u\frac{\partial v}{\partial x} + v\frac{\partial v}{\partial y}) = -\frac{\partial P}{\partial y} + \mu\nabla^2 v$$

As mentioned in above, a finite volume method has been used to solve the governing equations in this numerical simulation. For high accuracy of calculations, the discretization of convection and distribution terms was performed using second order method, and the SIMPLE algorithm was used too. It should be noted that due to the fact that the shape is geometrically

axisymmetric, then in order to reduce the computational volume of the model, the symmetric axial solver is used.

2.3. Turbulence Modeling

As the flow inside the jet is turbulent, therefore, a proper turbulent model should be considered for simulated model. The results of previous researches in this field suggest the well-known Standard k-ε turbulence model has better and closer to the experimental results than other models such as k-ω, SST, k-εRNG and RSM turbulence models [23]. In addition to the above equations, the equations related to the k-ε turbulence model must be solved simultaneously. These equations are as follows:

$$\rho \frac{\partial}{\partial t}(k) + \rho \frac{\partial}{\partial x i}(ku_i) = \frac{\partial}{\partial x j}[(\mu + \frac{\mu_t}{\sigma_k})\frac{\partial k}{\partial x j}] + G_k + G_b - \rho\varepsilon - Y_M \qquad (3)$$

$$\rho \frac{\partial}{\partial t}(\varepsilon) + \rho \frac{\partial}{\partial x i}(\varepsilon u_i) = \frac{\partial}{\partial x j}[(\mu + \frac{\mu_t}{\sigma\varepsilon})\frac{\partial \varepsilon}{\partial x j}] + C_{1\varepsilon}\frac{\varepsilon}{k}(G_k + C_{3\varepsilon}G_b) - C_{2\varepsilon}\rho\frac{\varepsilon^2}{k} \qquad (4)$$

In these equations, G_k, G_b and Y_M represent the turbulence kinetic energy production due to the mean velocity gradient, turbulence kinetic energy production due to the buoyancy force and contribution of velocity fluctuations in compressible turbulent flow respectively. σ_k and σ_ε represent the turbulence Prandtl number for k and ε respectively. $C_{1\varepsilon}$, $C_{2\varepsilon}$ and C_μ are constants: $C_{1\varepsilon} = 1.44$, $C_{2\varepsilon} = 1.92$, $C_\mu = 0.09$, $\sigma_k = 1.0$, $\sigma_\varepsilon = 1.3$

The turbulent viscosity μ_t is also calculated according to k and ε values as follows:

$$\mu_t = \rho C_\mu \frac{k^2}{\varepsilon} \qquad (5)$$

It is worth mentioning that the working fluid in this research is air with turbulence and incompressible (Ma<0.3) flow. The two dimensional and steady state condition governs the problem. In addition inlet pressure and temperature are set to 1 bar and 300 K respectively together with 1.4 bar for outlet pressures all similar to experimental conditions in Liu et al. [21].

2.4. CFD Calculations

CFD calculations are based on the numerical solution of continuity, momentum and turbulence equations for the incompressible flow. Since all simulations are performed at subsonic flow with a maximum Mach number of 0.3, the assumption of incompressibility is correct. All of the governing equations are discretized using the second order backward method. An implicit method is used to solve the governing equations. The rectangular computational domain of 28,000 cells has been used in simulations. In order to simulate the more precisely of the flow details, the size of the elements has dropped considerably near the entrance and near the jet axis, as sever gradients are expected in these areas.

In this model, the top and the bottom walls are stationary, and the right wall is flown to the environment as shown in Figure 2. In addition, primary and secondary inlets have been located on the left side of the jet. Also the dimensions of the present study have been shown in Figure 2.
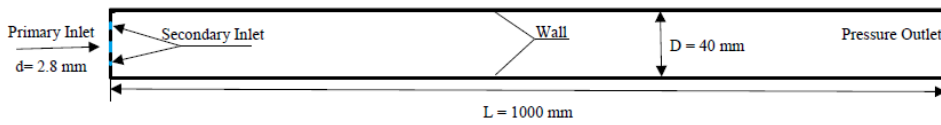
Figure 2. Simulated jet with boundary conditions

One of the most important parameters in this study is the ratio of secondary inlet mass flow rate ($\dot{m}_2$) to first inlet one ($\dot{m}_1$) which is called suction ratio (ω) and can be calculated from the following equation:

$$\omega = \frac{\dot{m}_2}{\dot{m}_1} \tag{6}$$

2.5. Grid Independence Study

To eliminate and reduce any errors due to the coarseness or inappropriate dimensions of the fluid field mesh and the independence of the analysis results from the effects of meshing, numerical modeling was conducted with different mesh sizes to investigate the effect of the number of meshes. For this purpose, eight models are made in the number of different elements and the results are based on the important parameter of the suction ratio and are shown in Fig. 3.
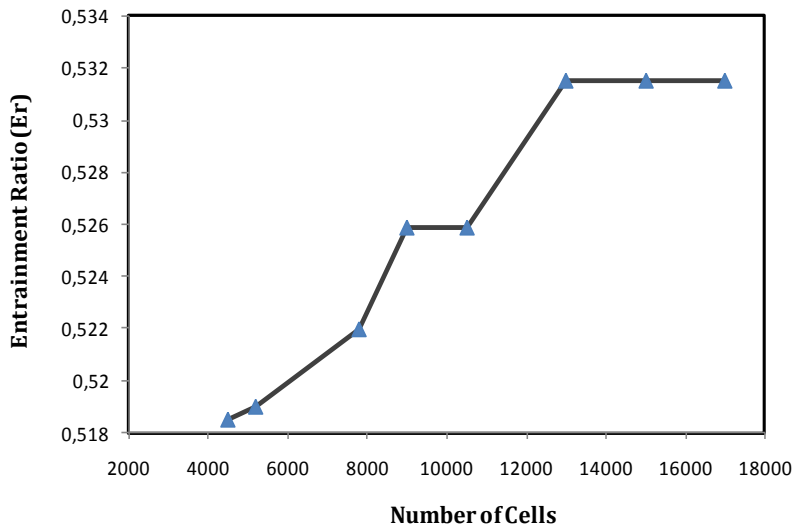
Figure 3. Grid independent study based on suction ratio (ω)

The definition of the suction ratio (ω) has been illustrated in Eq. 6. The results indicate that for a total number of more than 13,000 elements, the change in results is negligible. As a result, due to the stability of the results and the independence of the numerical results from the grid effects, the same number of elements is used to reduce the computational time for all models.

2.6. Validation

To compare the numerical results of the jet discharged into the tube with experimental results, the dimensionless velocity (u/U_m) versus dimensionless radial distance (r/R_u) from the tube

center, at x = 30d, and for a model d/D = 0.07 is depicted. R_u is where the velocity is half of the maximum velocity (u = $U_m/2$). Figure 4 shows the comparison between the experimental results [21] and the present numerical results that show an acceptable agreement between them.
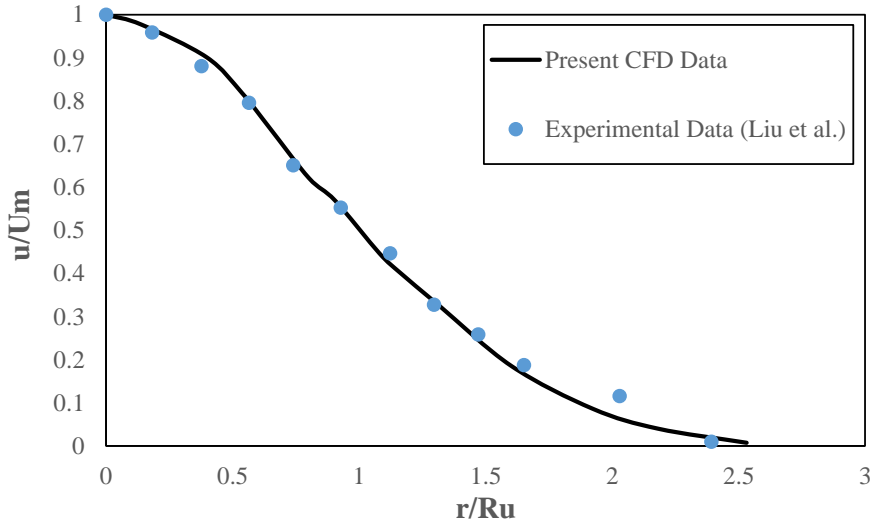
Figure 4. Comparison of present numerical results with experimental data [21]: A non-dimensional velocity in radial direction
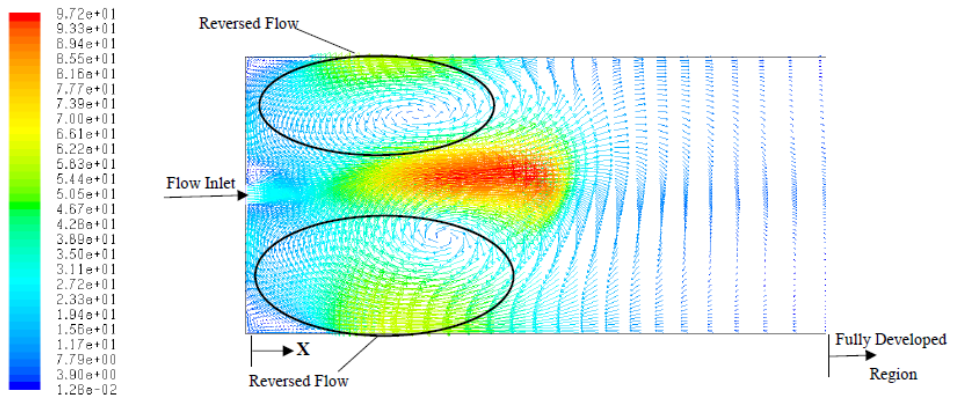
Figure 5. Velocity vectors at the beginning of the channel

Figure 5 shows the velocity vectors in the channel input and nozzle output area. As it can be seen, the turbulence of the flow and the presence of reversed flows in this area are quite evident. However, with the advance in the channel and reaching the developed area, the velocity profile becomes constant and does not change. Figure 6 shows the velocity vectors in the middle areas of channel. The results in this section are done for a jet with one inlet flow.
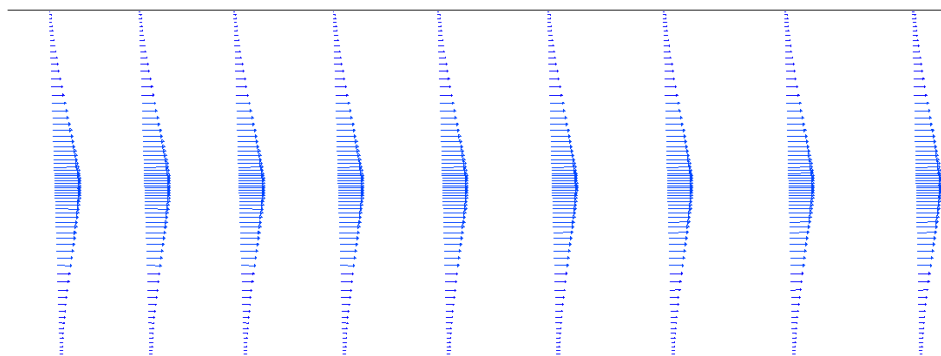
Figure 6. The velocity profile in the middle of the channel

2.7. Effect of secondary inlet on the jet flow

Now, after validation, the effect of creating the secondary inlet on the flow field and the secondary fluid suction volume are investigated. For this purpose, the value of r (the location of the secondary input) is changed. It is worth noting that the input thickness (Δr) must be changed so that the input area remains constant. So, different $\dfrac{\Delta r}{r}$ are evaluated in order to find a critical value $(\dfrac{\Delta r}{r})_c$ for which we have the highest amount of suction. For this purpose 3 different values of $\dfrac{\Delta r}{r}$ are studied here. These values are summarized in Tab. 1.

Figure 7 displays axial velocity contours for different case studies. As it can be seen, the flow core has been formed in the middle of the tube. Near the walls, there are reversed flows specially in the area of secondary inlet. This phenomenon has been shown in diagrams like Fig. 8. Axial velocity along centerline of the jet decreases as the flow moves forward in the jet in all models and becomes constant after reaches to developed region. In model with only one inlet, the length of developing region is shorter than models with one extra inlet.

Table 3. Different values of r (the location of the secondary input) and input thickness (Δr)

No.	r (mm)	Δr (mm)	$\dfrac{\Delta r}{r}$
1	10	6	0.6
2	20	3.6	0.18
3	38	2	0.05
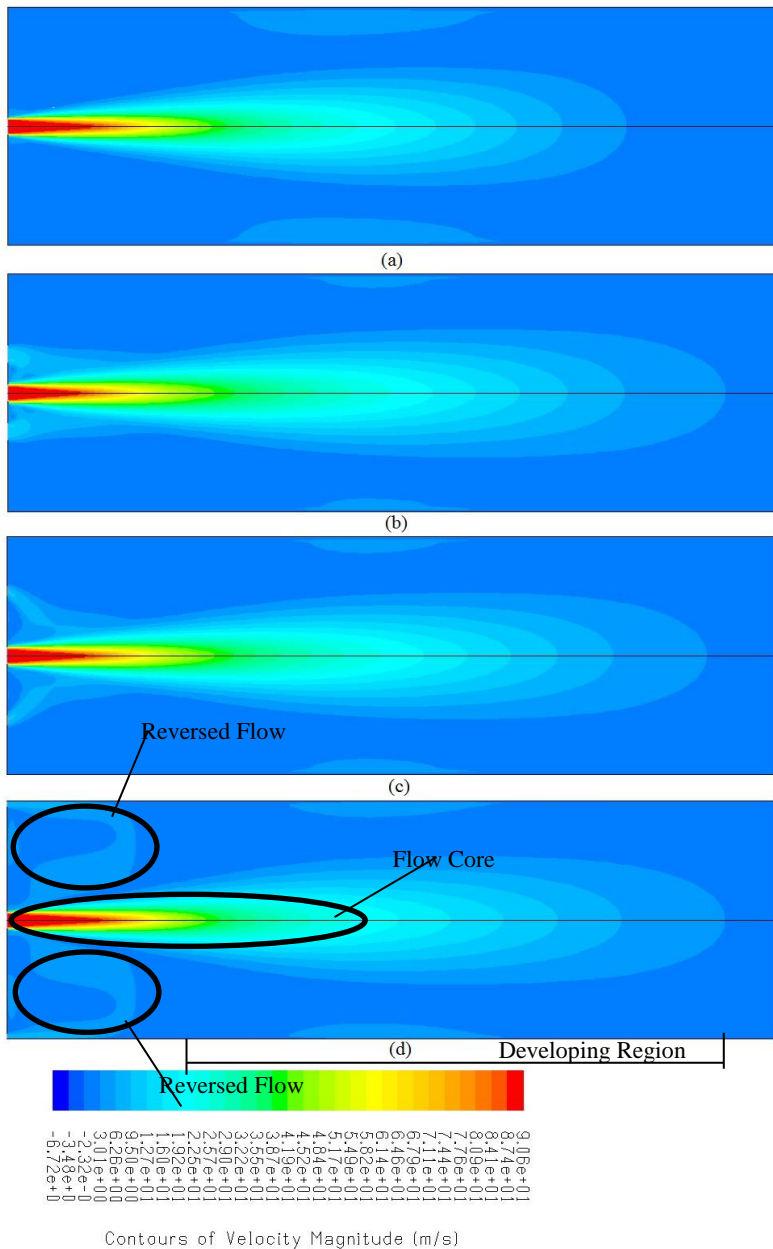
Figure 7. Axial velocity distribution inside jet with a) one inlet b) $\dfrac{\Delta r}{r} = 0.6$ c) c= 0.18 and d) $\dfrac{\Delta r}{r} = 0.05$.

Axial Velocity at x/R=1
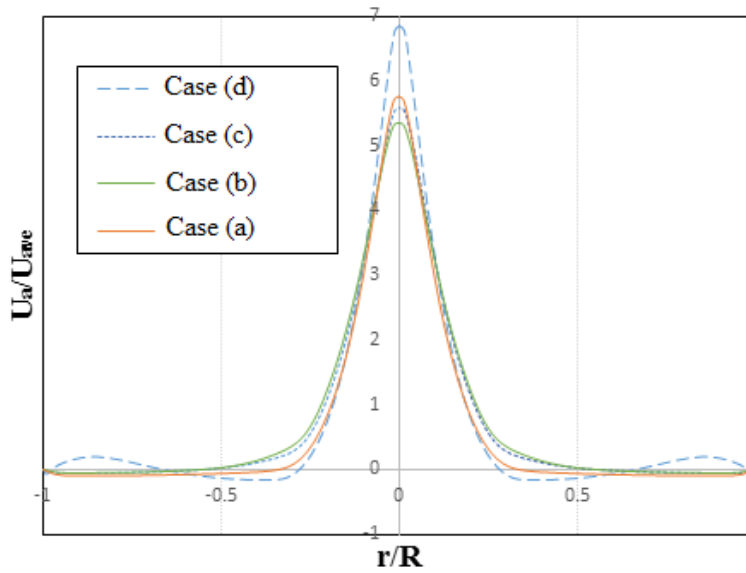
Axial Velocity at x/R=2
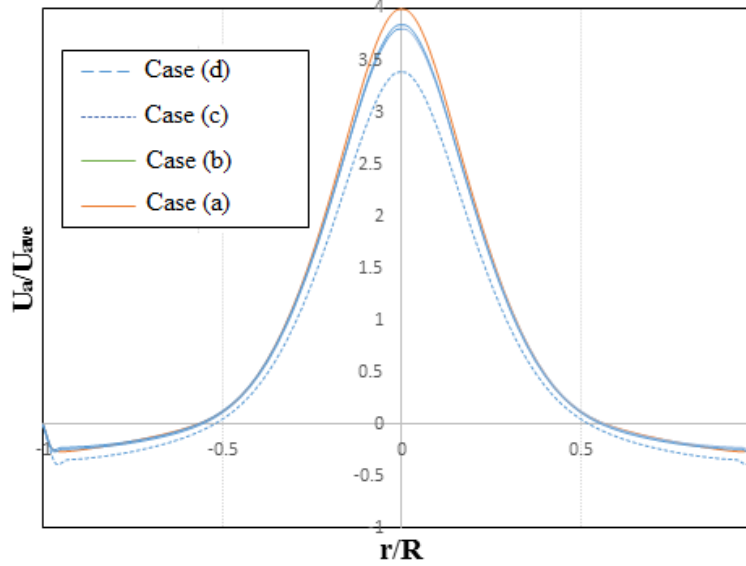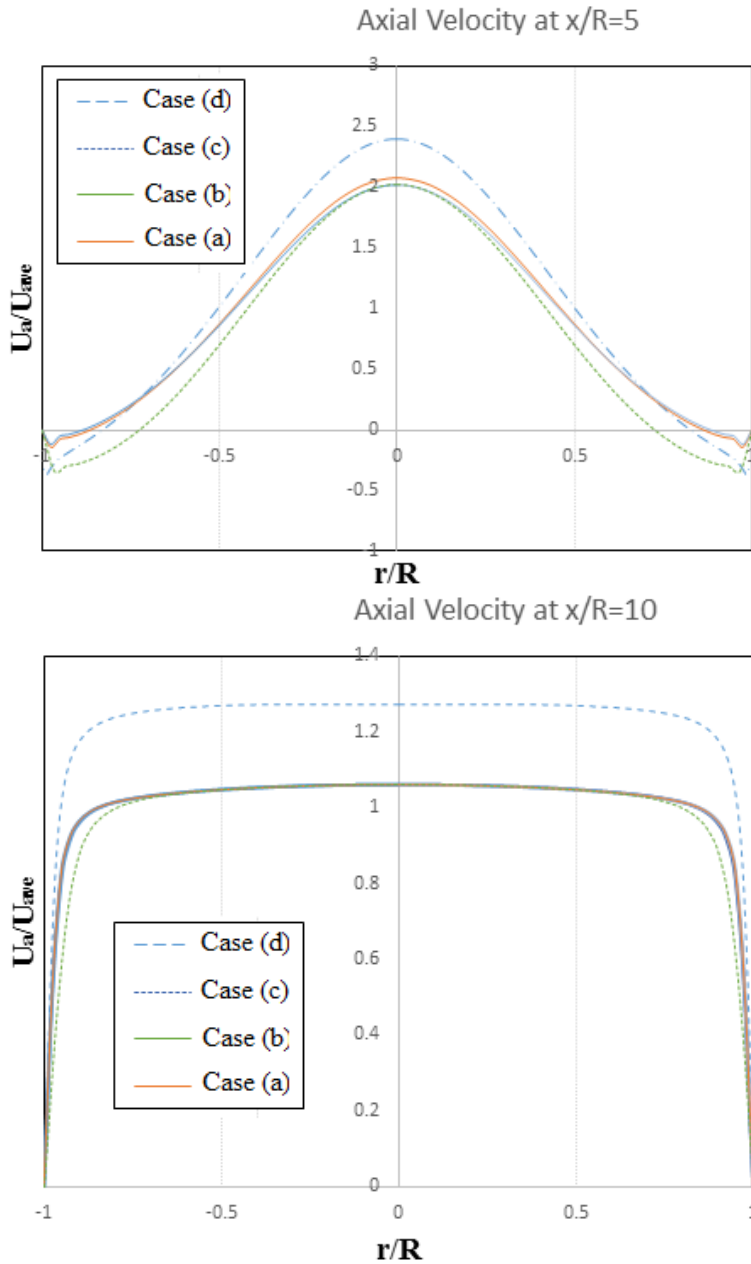
Figure 8. Dimensionless axial velocity profiles in different distances along dimensionless radius distances inside jet with a) one inlet b) $\dfrac{\Delta r}{r} = 0.6$ c) c= 0.18 and d) $\dfrac{\Delta r}{r} = 0.05$.

(a)

(b)

(c)

(d)

Contours of Static Pressure (atm)
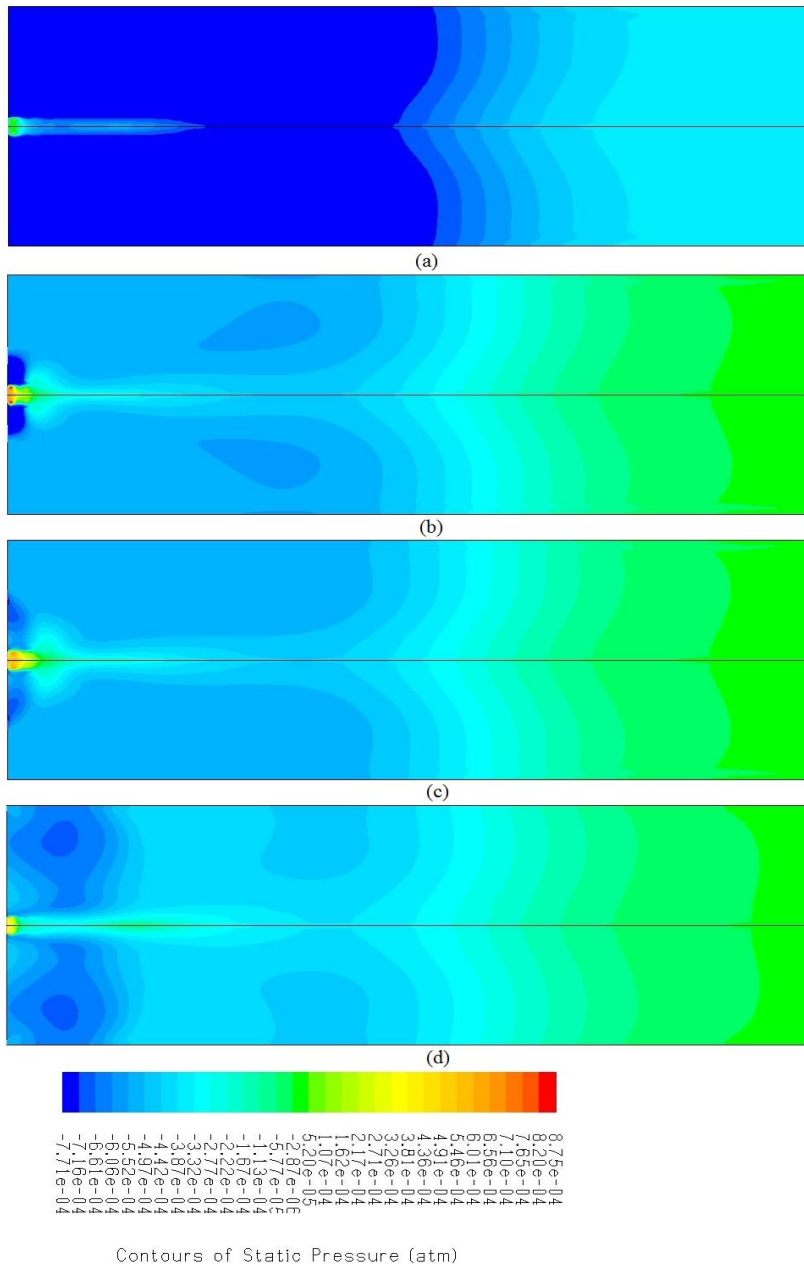
Figure 9. Static pressure distribution inside jet with a) one inlet b) $\dfrac{\Delta r}{r} = 0.6$ c) $\dfrac{\Delta r}{r} = 0.18$ and

d) $\dfrac{\Delta r}{r} = 0.05$.

As it can be seen, the number of vortices increases in jet as $\dfrac{\Delta r}{r}$ decreases. This phenomenon occurs due to the existence of a high pressure area in this area and causes the change in the flow pattern in the mixing region. The reason of this phenomenon is the low momentum of the secondary inlet fluid and, more importantly, the existence of a high pressure region, in the mixing region of two streams (Fig. 9). After flow passing the developing region, the reversed flows disappear and we will have a uniform flow. In addition, the area of reversed flows become smaller as $\dfrac{\Delta r}{r}$ decreases.

It is important to emphasize that vortices and their effects are complex. As a result of many of these complex parameters, estimating the vortex size can be difficult. It therefore requires sophisticated mathematical work in this field. This is discussed below.
Investigating the present jet showed that a linear equation can estimate the size of the vortices along the channel. This equation is expressed by Eq. (7).

$$\lambda = Cx \tag{7}$$

C is a dimensionless constant that is a function of $\dfrac{\Delta r}{r}$. This equation is approximate for different $\dfrac{\Delta r}{r}$. Determining the optimal value of the correction factor C is done by fitting the curve using the least squares error method on the CFD solution results as shown in Fig. 10. The proposed expression for function C is as follows:

$$C = 0.108 \, (\frac{\Delta r}{r})^2 + 1.8814 \frac{\Delta r}{r} + 3.623 \tag{8}$$
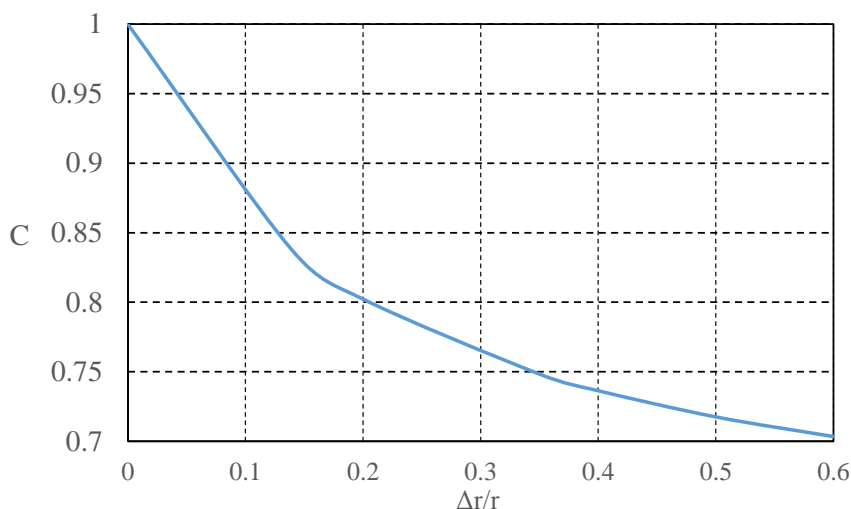
Figure 10. Determining the C function by fitting the curve to the CFD solution results for different simulated models

The above equation error is generally less than 7%. The results show that the secondary inlet influences the results such that changes both the size and the mode of vortex shedding change. However, by using the innovative method of this research and by using the appropriate suggestion of λ function; one can propose an appropriate expression for this function with the least squares error method and use it to determine the size of the vortices in terms of $\dfrac{\Delta r}{r}$.

Table 2 displays the suction ratios (ω) for different models in this study. As it can be seen the model with $\dfrac{\Delta r}{r}$ =0.6 has the greatest value of suction ratio i.e. 0.78. So this model is suggested for using in jet systems. Because the main duty of a jet in every system is to mix one fluid with another so how much the amount of suction is greater the greater amount of fluid can be injected to the system. Hence the greatest the suction ratio value, the better the perfomance of jet.

Table 2. Suction ratios for present models

$\dfrac{\Delta r}{r}$	$\dot{m}_1 \ (\dfrac{gr}{s})$	$\dot{m}_2 \ (\dfrac{gr}{s})$	ω
0	2.715	0	0
0.6	2.715	6.616	0.78
0.18	2.715	5.556	0.70
0.05	2.715	5.524	0.68

2.8. Effect of temperatures of primary and secondary inlet fluids on suction ratio

As shown in Fig. 11, with the increase of the primary fluid temperature, the suction ratio decreases, which means that the ratio of the amount of secondary fluid to the primary fluid decreases with increasing primary fluid temperature.
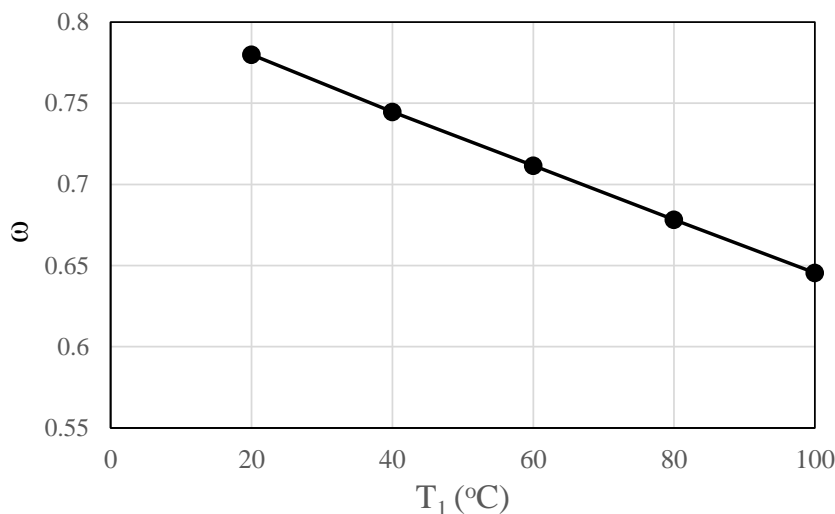
Figure 11. Suction ratios changes versus the initial fluid temperature

This result is logical because, with increasing temperature, the inlet mass flow rate of the primary fluid is increased. On the other hand, the pressure of the primary fluid increased relative to the state before it has lower temperature. Therefore, the pressure difference between the primary and secondary fluids in this situation decreases with the secondary fluid pressure and hence the mass flow rate is proportional to the pressure difference between the two inlet flows, therefore the secondary fluid mass flow rate decreases and does ω.

Another result of this simulation is the change in the suction ratio for different secondary temperatures as shown in figure 12. According to that, for the constant primary fluid temperature, ω increases with increasing secondary fluid temperature. This can be due to the greater difference in pressure between the secondary and primary fluids. In both of the above diagrams, with the increase of the primary and the secondary fluids, the pressure and temperature of the outlet flow from the jet increase, which can be explained by the energy conservation law.
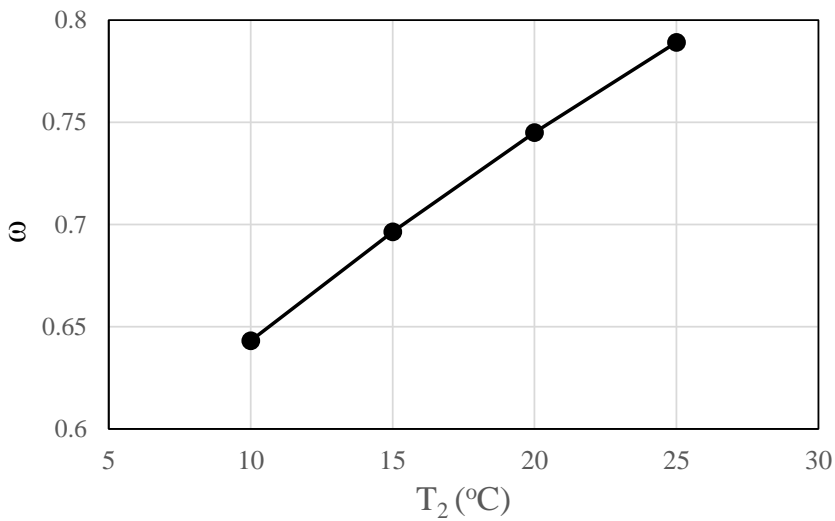
Figure 12. Suction ratios changes versus the secondary fluid temperature

2.9. The effect the compression ratio (P_3/P_1) on the suction ratio (ω)

The compression ratio is equal to the ratio of the pressure of the outlet fluid to the pressure of the primary fluid to the jet, and the results show that this ratio has a great influence on ω (Fig. 13). As shown in Fig. 13, increasing the compression ratio decreases the value of suction ratio. When compression ratio increases, the difference in pressure between the outlet and primary fluids is increased, it can be concluded that the difference between the total energy of the two fluids has increased. On the other hand, the primary mass fluid rate at a special temperature must be such as to compensate for the lack of secondary fluid energy, so the initial fluid with a higher mass rate should be fed into the jet. Alternatively, the secondary fluid must enters the jet with less mass, which means reducing the suction ratio.
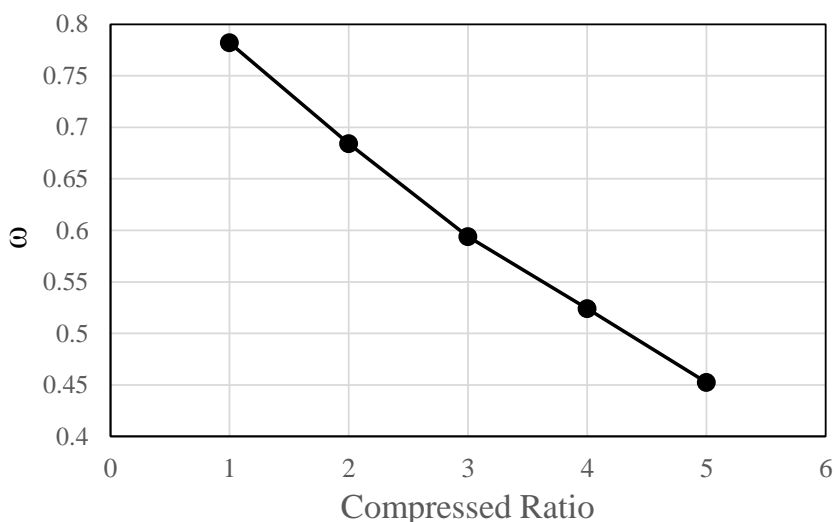
Figure 13. Suction ratios changes versus the compressed ratio

3. CONCLUSION

In present numerical study, using CFD technique, the effect of the key parameter of secondary inlet to a sample jet on the suction ratio, reversed flow due to the secondary input pressure and the effect of all these parameters on the fluid behavior, including speed and pressure were investigated. The fundamental flow equations of the flow field are solved by Fluent software and with a incompressible two-dimensional and standard k-ε turbulence model. The results were extracted and analyzed for different $\dfrac{\Delta r}{r}$. For this purpose, three different values of $\dfrac{\Delta r}{r}$ were investigated and compared to the jet with one inlet. The results indicated that for the $\dfrac{\Delta r}{r} = 0.6$, we have the highest amount of suction ratio in the device. A study was also carried out on the occurring of secondary flow inside the jet. According to that, reversed flows are evidence near the walls in the secondary inlet region. In the case where the geometry of the jet is constant, with the assumption that the jet outlet pressure is not constant, the suction ratio decreases with increasing primary fluid temperature. In contrast, as the secondary fluid temperature increases, the suction ratio increases too. Finally, the obtained results showed that increasing the compression ratio decreases the value of suction ratio.

Nomenclature

K	Turbulence kinetic energy (m^2/s^2)
$\dot{m}$	Mass flow rate (gr/s)
L	Length (mm)
d	Orifice diameter (mm)
D	Tube Diameter (mm)
g	Gravity acceleration (m/s^2)
Ma	Mach number

P	Pressure (Pa)
r	Radial distance from center (mm)
x	Axial distance from inlet (mm)
u	x-direction Velocity (m/s)
v	y-direction Velocity (m/s)
U_m	Maximum velocity (m/s)
R_u	Where the velocity is half of the maximum velocity (mm)
ε	Turbulence distribution rate (m^2/s^3)
ρ	Density (kg/m^3)
ω	Suction ratio
σ	Stress (N/m^2)
μ	Dynamics viscosity (kg/(m.s))
μ_t	Turbulence viscosity (kg/(m.s))
τ	Shear stress (N/m^2)
τ_{ij}	Stress tensor components

REFERENCES

[1]   Fitzgerald C., Oosthuizen J.C. and O'Dwyer T., (2014) A case of quinsy following high-pressure water jet injury, *Irish Medical Journal* 107,6, 178.

[2]   Polácek J. and Janurová E., (2017) Impact of pressure of surrounding medium on plain water jet cutting of rocks, *International Journal of Advanced Manufacturing Technology* 90, 2185–2191.

[3]   Kawanaka T., Kato S. and Kunieda M., (2014) Selective surface texturing using electrolyte jet machining, *Procedia CIRP* 13, 345-349.

[4]   Karimi Sadaghiyani O., Soufi Boubakran M., and Hassanzadeh A., (2018) Energy and exergy analysis of parabolic trough collectors, *International Journal of Heat and Technology* 36, 1, 147-158.

[5]   Chin, S.B., Foo, J.J., Lai, Y.L. and Yong, T.K.K., (2013) Forced Convective Heat Transfer Enhancement with Perforated Pin Fins, *Heat Mass Transfer* 49, 1447–1458.

[6]   Naphon, P., and Nakharintr, L., (2012) Heat Transfer of Nanofluids in the Mini-rectangular Fin Heat Sinks, *Int. Commun. Heat Mass Transfer* 40, 25–31.

[7]   Jasperson, B.A., Jeon, Y., Turner, K.T., Pfefferkorn, F.E. and Qu, W., (2010) Comparison of Micro-pin-fin and Microchannel Heat Sinks Considering Thermal-hydraulic Performance and Manufacturability, *IEEE Trans. Compon. Packag. Technol* 33, 148–160.

[8]   Forstall, W. and Shapiro A.H., (1950). Momentum and Mass Transfer in Coaxial Gas Jets, *Journal of Applied Mechanics* 18, 2, 399-408.

[9]   Starck P., (2007) Prediction of Flame Lift off Height of Diffusion/Partially Premixed Jet Flames and Modeling of Mild Combustion Burners, *Combustion Science and Technology* 179, 10, 2219-2253.

[10]   Morton B.R., (1962) Coaxial Turbulent Jets, *International Journal of Heat and Mass Transfer* 5,10, 955-965.

[11]   Chigier N.A. and Beer J.M., (1964) The Flow Region Near the Nozzle in Double Concentric Jets, *Journal of Basic Engineering* 86,4, 797-804.

[12]   Ghodsian M., Mehraein M. and Ranjbar H.R., (2012) Local scour due to free fall jets in non-uniform sediment, *Scientia Iranica* 19, 6, 1437-1444.

[13]   Champagne F.H. and Wygnanski I.J., (1971) An Experimental Investigation of Coaxial Turbulent Jets, *International Journal of Heat and Mass Transfer* 14, 9, 1445-1464.

[14] Ribeiro M.M. and Whitelaw J.H., (1976) Turbulent Mixing of Coaxial Jets with Particular Reference to the Near-Exit Region, *Journal of Fluids Engineering-Transactions of the ASME* 98, 2, 284-291

[15] Ko N.W.M. and Kwan A.S.H., (1976) The Initial Region of Subsonic Coaxial Jets, *Journal of Fluid Mechanics* 73, 2, 305-332.

[16] Dahm, W.J.A., Frieler C.E. and Tryggvason G., (1992) Vortex Structure and Dynamics in the Near Field of a Coaxial Jet, *Journal of Fluid Mechanics* 241, 371-402.

[17] Buresti, G., Petagna P. and Talamelli A., (1998) Experimental Investigation on the Turbulent Near-field of Coaxial Jets, *Experimental Thermal and Fluid Science* 17, 18-26.

[18] Warda H.A., Kassab S.Z., Elshorbagy K.A. and Elsaadawy E.A., (2001) Influence of the Magnitude of the Two Initial Velocities on the Flow Field of a Coaxial Turbulent Jet, *Flow Measurement and Instrumentation* 12,1, 29-35.

[19] Schumaker S.A., (2009) An Experimental Investigation of Reacting and Nonreacting Coaxial Jet Mixing in a Laboratory Rocket Engine, *Ph. D. thesis, University of Michigan,* Ann Arbor, Michigan, USA.

[20] Zhuang Y., M, C.F. and Qin M., (1997) Experimental study on local heat transfer with liquid impingement flow in two-dimensional micro-channels, *Int. J. Heat Mass Transfer* 40, 4055–4059.

[21] Liu H., Winoto S.H. and Shah D.A. , (1997) Velocity Measurements within Confined Turbulent Jets, *Application to Cardiovalvular Regurgitation. Annals of Biomedical Engineering* 25, 939-948.

[22] Hassanzadeh, A., Pourmahmoud N. and Dadvand A., (2017) Numerical simulation of motion and deformation of healthy and sick red blood cell through a constricted vessel using hybrid lattice Boltzmann-immersed boundary method, *Computer methods in Biomechanics and Biomedical engineering* 20,7, 737–749.

[23] Pourmahmoud N., Rashidzadeh M. and Hassanzadeh A., (2015) CFD investigation of inlet pressure effects on the energy separation in a vortex tube with convergent nozzles, *Engineering Computations* 32, 5, 1323-1342.

[24] Khodayari Bavil A. and Razavi S.E., (2017) On the thermo flow behavior in a rectangular channel with skewed circular ribs, *Mechanics & Industry* 18, 2, 225.